Int. J. Solids Structures Vol. 27, No. 8, pp. 1047–1058, 1991
Printed in Great Britain.

0020-7683/91 $3.00+.00

FINITE ELEMENT ANALYSIS OF CONE INDENTATION

A. K. BHATTACHARYA† and W. D. NIX‡
† Department of Mechanical Engineering and ‡ Department of Materials Science and Engineering, Stanford University, Stanford, CA 94305, U.S.A.

(*Received* 12 *April* 1989; *in revised form* 25 *April* 1990)

Abstract—An elastoplastic analysis of axisymmetric conical indentation has been made using the finite element method. Studies of the shapes of plastic zones and the effects of shear modulus, bulk modulus and indenter angle on the hardness of hard and soft materials have been made. The results show that the shapes of the plastic zones depend strongly on both indenter angle and the ratio of Young's modulus to yield strength (E/σ_y). It is also found that the bulk and shear moduli have large effects on the hardness of hard and soft materials, respectively.

INTRODUCTION

While a great deal of effort has been made to gather information on indentation processes through experiments, there is still a considerable lack of understanding of the detailed deformation processes occurring in an indentation test. This is especially true in cases of very small scale indentations. Understanding the mechanical properties in fundamental terms is particularly important in the application of sub-micron indentation techniques to thin films. Theoretical analyses of general indentation problems have received attention from various investigators since Prandtl (1920) developed a slip line field solution for a flat punch on a semi-infinite medium. From that time, the idea of hardness as a material property for the resistance to local deformation has been widely accepted. A detailed theoretical analysis of a flat punch indentation under plane strain conditions was given by Hill *et al.* (1951), and Shield (1955) obtained a similar solution for axisymmetric indentation by a flat circular punch. These theoretical solutions apply to rigid plastic materials and are based exclusively on the slip line method. Later, Lockett (1963) performed a numerical study of cone indentation based on the slip line theory. The same approach has also been used by Ishlinsky (1944) to obtain a solution for spherical indentation. Besides studying flat punch indentation, Hill *et al.* (1947) also considered wedge indentation under plane strain conditions. In constructing the slip line fields used in the above theories, the development of the plastic zone under the indenter is generally approximated from experimental observations.

Another line of approach to understanding indentation is semi-empirical in nature. Tabor (1970) gave an excellent review of the hardness of solids in which he developed a correlation between the mean contact pressure associated with indentation and the yield stress. To describe this correlation, he adopted the model of Marsh (1964) who, following Bishop *et al.* (1945), analyzed the plastically deformed zone as the expansion of a spherical cavity in an elastic–plastic solid with an internal hydrostatic pressure. Later, Johnson (1970) extended this approach to include the effect of the indenter geometry. His formulation provides the most comprehensive description of the correlation between experimental results on hardness and this approach. Rubenstein (1981) gave a review of these various semi-empirical approaches to indentation hardness.

In spite of these analyses, detailed solutions of indentation problems for realistic stress–strain relations and indenter shapes are still lacking because of the very complex stress and strain fields produced by these indentations. In fact, the simplified picture of the slip line fields often falls short of describing the actual plastic zones involved, even for the assumed rigid-plastic material property. Also, the spherical cavity expansion model has its limitations in that it cannot be applied to materials with high E/σ_y ratios and for indenters with small included angles. Plasticity solutions must be known in these cases to understand the physical

meaning of indentation hardness. Since the plastic deformation involved in an indentation depends on the path through which the current state is reached, it becomes necessary to consider the changes in deformation history continuously. Lee *et al.* (1970, 1972) used the finite element technique to analyze some aspects of flat punch and spherical indentations. Recently, Bourcier *et al.* (1985) also made simulations of some indentation problems using this method. Except for their study, analyses of very small scale indentations have not been made. The problem considered in the present study corresponds to an elastic and plastic analysis of cone indentation related to a typical micro-hardness test. Information about cone indentation experiments can be found in the literature (Atkins and Tabor, 1965; Dugdale, 1954), but the impressions made in these experiments are all comparatively large and hence some of the experimental information, especially the development of plastic zones, which is a key factor in the slip line analysis, needs to be re-examined for the case of small indentations. From the perspective of both the slip line theory and the spherical cavity model, the understanding of how the plastic zones develop is critical. It would be extremely difficult to study experimentally the development of plastic zones in sub-micron indentations. We have thus resorted to the finite element technique for such an analysis. It has been demonstrated that this method successfully describes micro-indentation processes in bulk materials (Bhattacharya and Nix, 1988a) and also for thin films on substrates (Bhattacharya and Nix, 1988b). In the following, we have analyzed the mechanics involved in cone indentations on a half space. We have studied the development of plastic zones and critically examined the applicability of the spherical cavity model and the slip line theory to such small scale indentations.

FINITE ELEMENT MODEL

Simulations of the force–distance relations for the sub-micron indentation of a half space using a rigid indenter were performed using the large strain elastoplastic feature of the ABAQUS finite element code (1985), with uniaxial stress-strain data as input. Materials with various yield stresses and Young's moduli were studied. The quasi-static nature of the process permits us to use the static analysis performed by the program. Underlying the approach in this code is the discretization of the continuum involved. The indenter was considered to be perfectly rigid and various indenter angles were considered. Also, an important feature of this program involves the capability to model contact between the indenter and the sample as a sliding interface. The initial nodal gaps between the indenter and the surface of the specimen were prescribed and the program automatically keeps track of their change and indicates any gap closure or opening in a particular specified direction. These interface elements thus simulate contact between the indenter and the specimen surface. Whenever the closure distance between the indenter and the specimen becomes zero, contact is assumed and an external reaction force is exerted on this material point to keep it moving along with the indenter. Because the program calls for incremental loading and also makes use of interface elements, the expanding contact area associated with indentation occurs naturally whenever new interface elements come into contact.

In this analysis, indenters having conical shapes have been considered and the specimen is treated as body of revolution. Under test conditions, the indenter tip will amost invariably have a finite radius, thus giving rise to a somewhat different response. The indenter and half of the specimen are shown schematically in Fig. 1, along with the appropriate boundary conditions for the problem. Symmetry properties have been used to simplify the boundary conditions. During preliminary simulations the boundary condition on the surface on the right side of the specimen was changed from fixed radial displacements to traction free; this change had no effect on the indentation parameters, thus showing that this boundary was indeed remote. Since very small indentations were being simulated, the meshes near the indenter needed to be very fine to be able to describe the deformation and stress gradients associated with indentation with sufficient accuracy. Thus, extremely fine mesh sizes were used under the indenter; they became progressively coarser at distances further away from the indenter. Axisymmetric four-noded elements were used for the continuum. Although higher order elements could have been considered to assure better accuracy, use of these

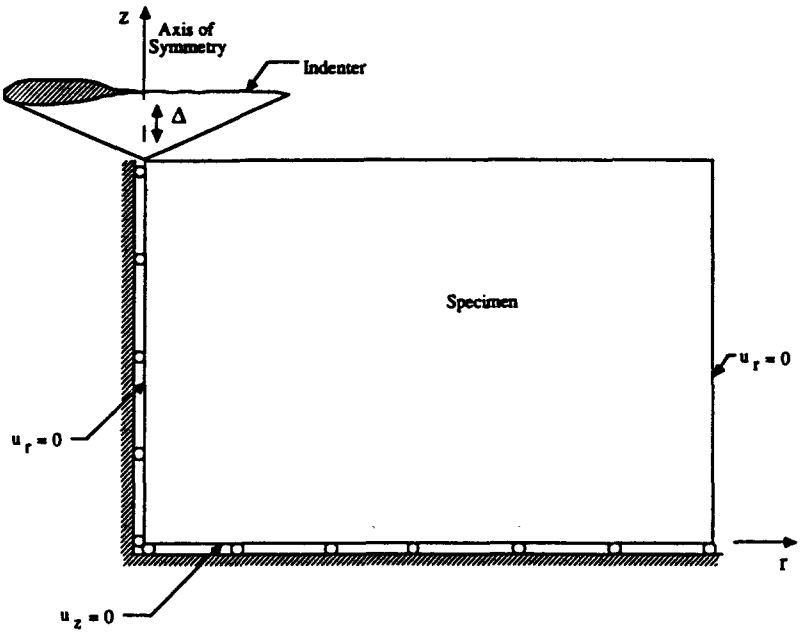

Fig. 1. Schematic diagram of the specimen under the indenter showing the boundary conditions of the problem.

four-noded elements is justified since it dramatically reduces the computation time while maintaining enough accuracy, as demonstrated by the close match with experimental results (Bhattacharya and Nix, 1988a). For an intricate problem such as indentation, having a single finite element solution is not sufficient to prove convergence. In general, we must repeat the solution process using a finer grid and compare the two solutions. As reported elsewhere (Bhattacharya and Nix, 1988a), we must continue to refine the grid until the divergence between two consecutive solutions is negligible. The grid refinement for the indentations reported in the present paper was such that the common nodal loads were essentially independent of further grid refinement.

In order to obtain an accurate estimate of the radius of the contact area, an extremely fine mesh thickness of the order of 0.02 μm had to be used along most of the indenter contact surface. To keep the required computer time within limits, a total of 461 elements including the interface elements were used to represent the deformed material. Figure 2 represents a magnified view of the elements near the indenter and the staircase arrangement for the other elements at points further away from the indenter. In this distribution of elements, when two elements are connected to a single element the middle node on the common face is constrained to lie on a straight line defined by the two corresponding end nodes.

To simulate a typical indentation process, a downward displacement (negative z-direction in Fig. 1) was imposed on the indenter; this causes the indenter to push into the surface of the material. Subsequently, the indenter was given an upward displacement until it was free of contact with the specimen. For a given indenter displacement, the corresponding load was found by summing the reaction forces at the contact node points on the indenter. The interface between the specimen and the indenter was assumed to be frictionless since no noticeable change in the load–displacement response was observed by using a friction coefficient of 1 for the cases with large angle indenters. This would not necessarily be true for the cases of very small angle indenters, because of the cutting action involved in such indentations. For the purpose of calculating an average hardness, the mesh thickness of 0.02 μm along the indenter contact surface was found to provide sufficient contact area for indenters having large angles, but it was necessary to make larger indentations for indenters with smaller included angles using the same mesh sizes.

With respect to convergence following each displacement increment, we have both doubled and halved the size of the displacement increment in the range of commonly used

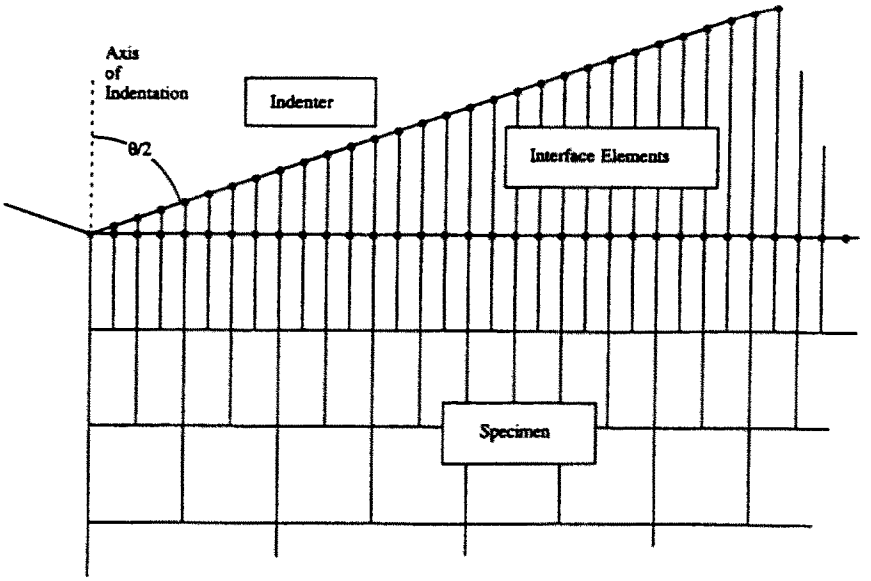

Fig. 2. Detailed pattern of the mesh distribution near the indenter showing the interface elements.

displacement increments; we find the resulting nodal forces to be unaffected by the size of the displacement increments. These checks were made for both soft and hard materials, e.g. aluminum and silicon, respectively. Also, the load convergence was checked by using an automatic displacement increment mode and comparing the nodal load values at the matching displaced points. In all cases, essentially exact load values were obtained.

The constitutive model for the specimen material was that of an elastic–plastic von Mises material. Two separate cases of strain hardening were considered, one with no strain hardening (i.e. the material was assumed to be elastic–fully plastic) and the other with a linear strain hardening rate of approximately $\mu/200$ for the material under consideration. Elastic and plastic properties of the material used in the various calculations are given as an inset in Fig. 3 and the relevant parameters are defined in Figs 3 and 4. The finite element calculations were performed using an IBM 4341 mainframe computer with runtimes of 1–2 days and also using a Vax II Workstation with runtimes of 5–6 days for average indentation depths.

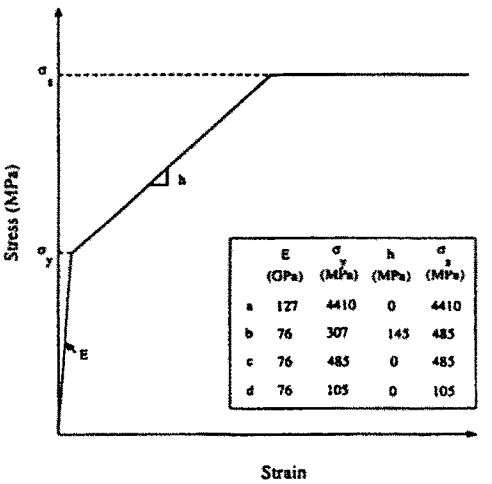

Fig. 3. Schematic diagram showing the stress–strain relations for the materials used in the FEM calculations.

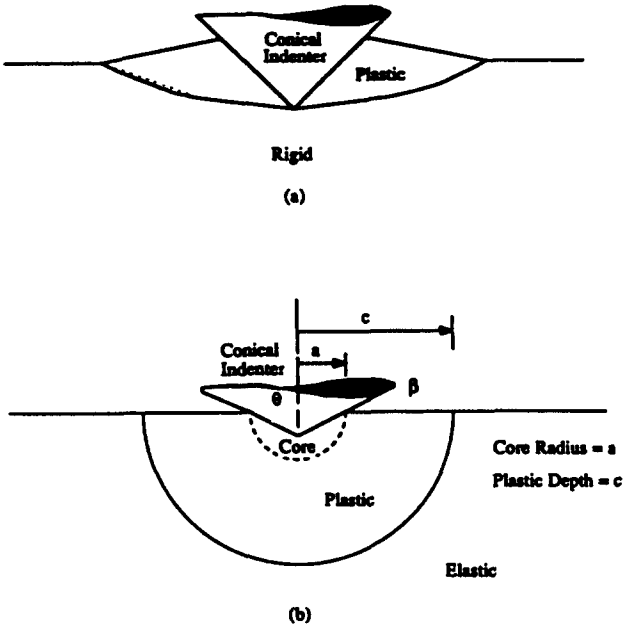

Fig. 4. Schematic representation of the yield zones for the slip line theory (a) and the spherical cavity model (b).

RESULTS AND DISCUSSION

Relationship between hardness, Young's modulus and yield strength

As indicated before, the solution utilizing the slip line field for a rigid plastic material considers only plasticity aspects of deformation without any elastic deformation or strain hardening effects. This particular approach is thus expected to be applicable for materials with high E/σ_y ratios and small indenter angles. The most comprehensive description of elastic–plastic effects for shallow indentations is due to Johnson (1970), who derived a relationship between hardness, yield strength and Young's modulus for the indented material, based on the spherical cavity expansion model in an infinite elastic–plastic solid. In Fig. 5 we show the hardnesses calculated using the FEM analysis for materials having different values of E, σ_y and ν. Also shown are the experimental results from Johnson (1970) and the predictions of the Johnson model for an incompressible material, $\nu = 0.5$. The FEM analysis predicts an upper bound to the experimental results and also describes the plateau

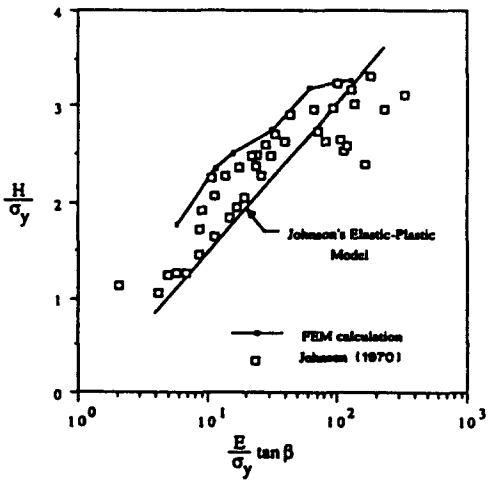

Fig. 5. Comparison of various experimental hardness measurements (Johnson, 1970) with the predictions of Johnson's elastic–plastic model and the present FEM analysis.

behavior at large values of E/σ_y, whereas the spherical cavity model seems to predict a lower bound to the experimental observations and does not appear to be applicable to materials having large values of $(E/\sigma_y \tan \beta)$. Moreover, by considering elastic compression under the indenter, the hardness predicted by the FEM analysis would be expected to be smaller and in better agreement with experimental results.

The applicability of Johnson's model is based on the assumption that the mode of deformation during indentation is one of radial compression caused by the hydrostatic stress beneath the indenter. According to this model, the hardness of an indented material is given as

$$\frac{H}{\sigma_y} = \frac{2}{3}\left(1+3\ln\frac{c}{a}\right) \tag{1}$$

where c and a are the radius of plastic zone and radius of the indented area, respectively. The relationship between c and a is described below with reference to Fig. 4. This model assumes that the deformed zone is hemispherical in shape. This has been observed experimentally by Samuels and Mulhearn (1957) for indentation of work hardened material with spherical and pyramidal indenters having large angles. In their observations, the hemisphere appeared to be centered slightly under the point of indentation as compared to the idealized center on the surface of the specimen as assumed in the spherical cavity model. In the slip line theory, the theoretical treatment is concerned with the boundary between the material which is plastically deformed and the material which has remained rigid. In the spherical cavity model, the boundary is between the plastic and elastic part of the material. The yield zones described by these models are shown schematically in Fig. 4. The extent of the plastic zone in the cavity model of Johnson (1970) is described as

$$\frac{c}{a} = \left[\frac{1}{6(1-\nu)}\left\{\frac{E}{\sigma_y}\tan\beta + 4(1-2\nu)\right\}\right]^{1/3} \tag{2}$$

where β is the inclination of the indenter. However, as we will see below, the shape of the deformed zone depends on the ratio E/σ_y and the indenter angle.

Figure 6 shows the development of the plastic zones for silicon and aluminum using a smooth indenter with an included angle of 136°. In this case of wide angle indenters, the deformed zones differ considerably from those assumed by the slip line theory. The deformed zones for aluminum ($E/\sigma_y = 157.3$) seem to resemble the hemispherical form assumed in the spherical cavity model but those for silicon ($E/\sigma_y = 27.8$) appear to have shapes that are between the hemispherical and cylindrical shapes. Also, for the case of silicon, the width of the deformed zone extends only up to the edge of the contact surface, in contrast to the

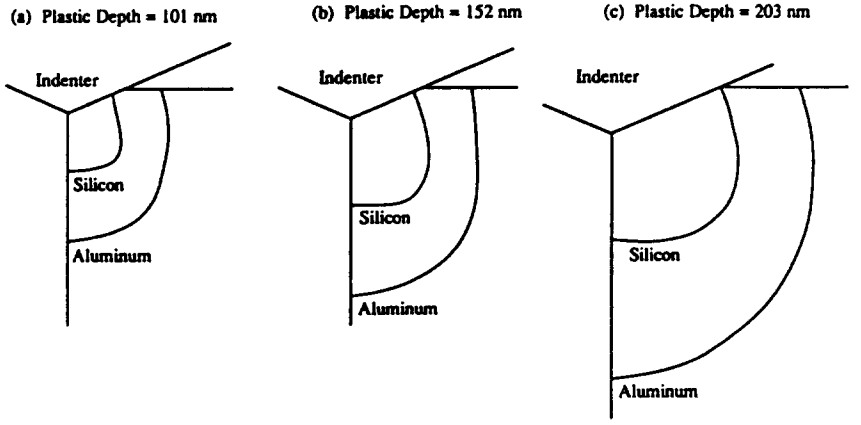

Fig. 6. Development of plastic zones associated with the indentation of silicon and aluminum.

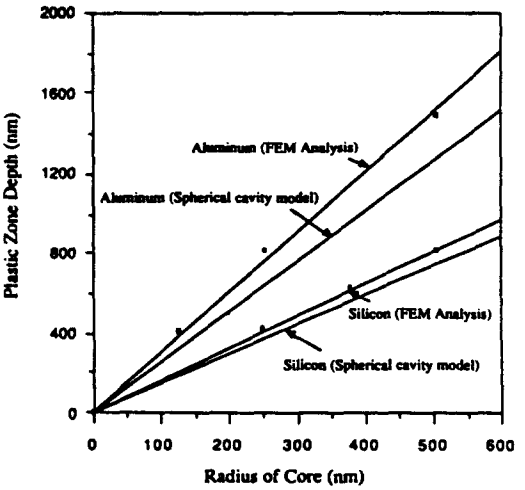

Fig. 7. Development of yield zones in silicon and aluminum.

larger radius predicted by the spherical cavity model. In Fig. 7 we have plotted the plastic depths as a function of the contact radius (defined in Fig. 4b) and compared the results with the predictions of the Johnson model [eqn (2)] using appropriate values of Poisson's ratio. Surprisingly, in spite of the different plastic zone shapes for silicon, the plastic depth closely matches that predicted by the spherical cavity model. The plastic zones for aluminum also match reasonably well with the predictions from the model, although for both materials the plastic depths are larger than those calculated from the spherical cavity model and this corresponds to the increased values of hardness calculated by the FEM analysis in Fig. 5.

Figures 8 and 9 show the stress distributions along the indenter surface for aluminum and silicon respectively. In both of these plots, the normal stresses are compressive. For the case of silicon, the compressive stress steadily decreases toward the elastic–plastic boundary (Fig. 9) whereas this stress remains fairly constant in the case of aluminum (Fig. 8). It is to be noted here that both the slip line theory and the spherical cavity model require the pressure distribution under the indenter to be uniform. For purely elastic deformation in cone indentations, the normal stress distribution (Sneddon, 1951) is given by

$$p = \frac{E \tan \beta}{2(1-\nu^2)} \cosh^{-1}\left(\frac{a}{r}\right) \tag{3}$$

where $2a$ is the indentation diameter and r is the radius from the centerline of the indenter.

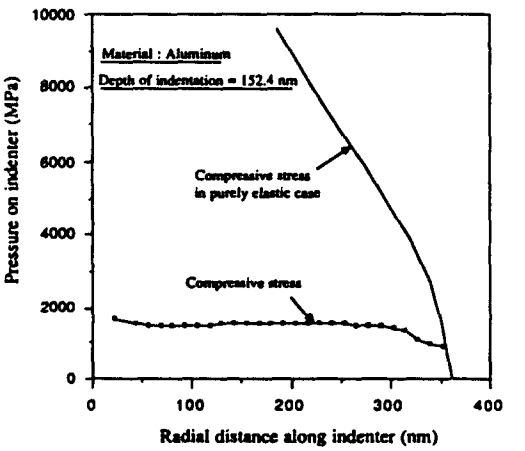

Fig. 8. Distribution of the compressive stresses in aluminum on the surface of the indenter and comparison with the case of elastic deformation only.

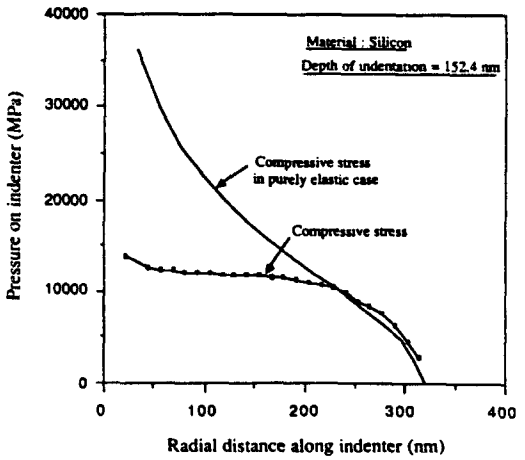

Fig. 9. Distribution of compressive stresses in silicon on the surface of the indenter and comparison with the case of elastic deformation only.

This stress distribution for purely elastic deformation is also shown in Figs 8 and 9. One finds that towards the outside region of the indenter, the calculated normal stress distribution for silicon is similar to this type of elastic distribution in that region, indicating the elastic–plastic nature of deformation in this case. For the case of aluminum, however, the distribution of normal stress from FEM calculations is totally different both in magnitude and in trend from those of the purely elastic case across the whole width of the indenter, thus indicating the dominance of plasticity under the indenter. This plasticity effect indeed causes the yield zone to spread well beyond the end of the contact point as seen in Fig. 6. Figures 10 and 11 represent the stress distribution along the axis of indentation. Again, all of the stress components are compressive and a large hydrostatic pressure is evident in the case of silicon indentation (Fig. 11).

As a check on the methods used to calculate the pressures under the indenter we have calculated the distribution of pressure under a cone indenter on an elastic half space and compared the results with eqn (3). The agreement found was very close and the asymptotic behavior was observed in the FEM solution. Only at the two or three elements nearest the indenter tip did the FEM solution begin to fall short of the predictions of eqn (3). These errors are insignificant, however, when one considers that the number of contacting elements is at least 10 times greater than the number of elements where the error is detected, even for the smallest indentations studied; larger indentations involve even more elements.

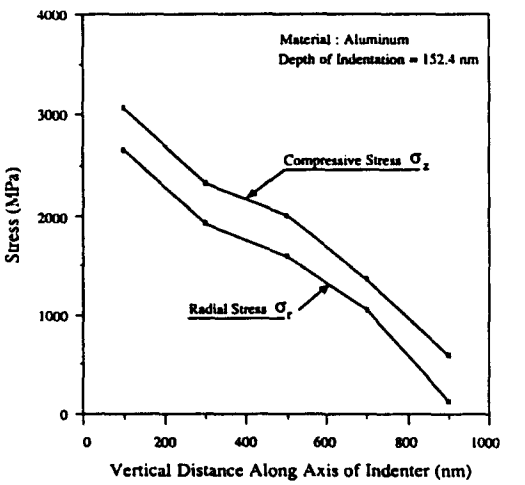

Fig. 10. Stress distribution in aluminum along the axis of indentation.

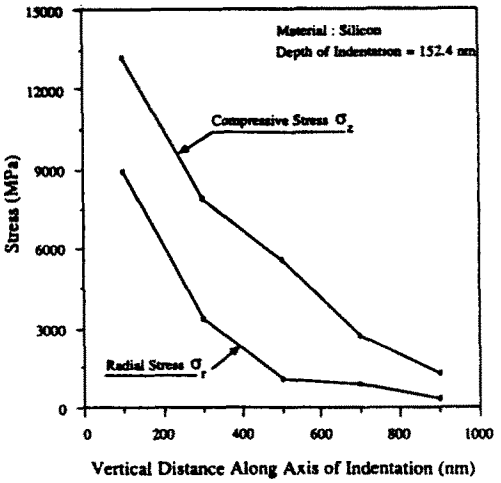

Fig. 11. Stress distribution in silicon along the axis of indentation.

Effect of bulk and shear moduli

Because indentation hardness involves plasticity, the hardness depends in part on the yield strength of the material. But the material under the indenter is also subjected to a large pressure, which results in elastic compression of the material being indented. The response of a material to hydrostatic pressure is given by its coefficient of elastic compressibility expressed as the bulk modulus of the material. On the other hand, the shear modulus represents a measure of the shear rigidity of a material. Thus, both elastic compression and shear rigidity should influence the hardness of the material. In Fig. 12 we have plotted H/σ_y values against $\log[\{4(1-2\nu)+E\tan\beta/\sigma_y\}/6/(1-\nu)]$. This should be a straight line according to Johnson's spherical cavity model. In this plot we have also shown FEM calculations for the indentation of silicon and aluminum with three different combinations of Young's modulus and Poisson's ratio. Data points 1, 3 and 5 represent silicon and 2, 4 and 6 represent aluminum. Points 1 and 2 are for the usual values of E and ν for the respective materials. Points 3 and 4 represent a 2.5 and 3 fold increase in the bulk modulus values for silicon and aluminum, respectively, while maintaining the respective shear modulus values constant. Similarly, points 5 and 6 represent a 2.5 and 3 fold increase in the shear modulus values for silicon and aluminum, respectively, while the respective bulk modulus values are kept constant. We have also plotted the hardnesses with these E and ν values according to Johnson's cavity model which, as expected, fall on a straight line. It is observed that Johnson's model only implicitly considers the effect of bulk and shear moduli through E and ν and thus fails to indicate the separate effects of the shear and bulk moduli on the

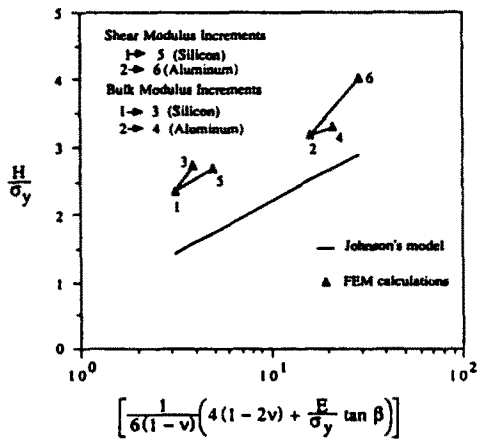

Fig. 12. Effect of shear and bulk moduli on the hardness of silicon and aluminum.

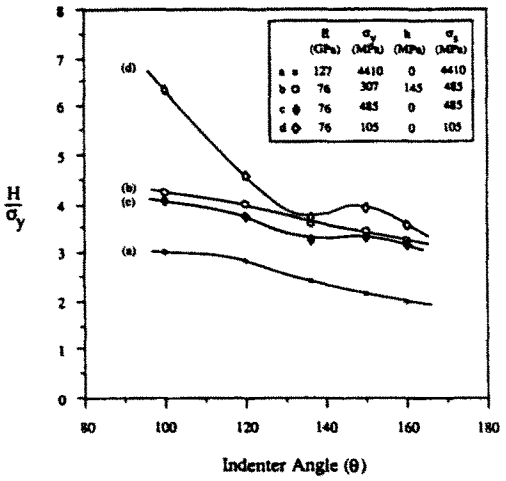

Fig. 13. Effect of indenter angle on the hardness for materials with different stress–strain relations.

hardness of different types of material as shown by the FEM results. As discussed before, in this plot it is indeed seen that the effect of changing the bulk modulus is more important than changing the shear modulus for a hard material like silicon, whereas for aluminum, which is a soft material, a larger effect is observed for the change in the shear modulus. The presence of a large hydrostatic pressure for indentation of silicon is also observed in Fig. 11, which is consistent with this prediction of the effect of the bulk modulus.

Effect of indenter angle and work hardening on hardness

Atkins and Tabor (1965) made hardness measurements on copper with various states of work hardening using conical indenters having widely different angles. Their experiments show that for fully annealed material, the hardness continuously drops from a large value at small cone angles to smaller values at larger cone angles, whereas for fully work hardened material, the hardness reaches a minimum value, after which it increases at larger cone angles. For other states of work hardening, the hardness values lie between these two extremes. We have analyzed the effect of indenter angle on four different types of material whose stress–strain characteristics are schematically shown in Fig. 3. In Fig. 13 the calculated values of H/σ_y are plotted against cone angles between 100° and 160° for materials with different yield stresses, elastic moduli and strain hardening properties. The values of E/σ_y range from 28.8 for silicon to 733.3 for silver. It is observed that for the material with a low E/σ_y value, i.e. for the hardest material (curve a), the H/σ_y value continuously decreases with increasing indenter angle. The same trend is also seen for the fully annealed material (curve b). This observation about the fully annealed material is consistent with the experimental observations of Atkins and Tabor as described earlier. However, for a material without strain hardening and with a high E/σ_y ratio (curve d), H/σ_y reaches a minimum after which it again increases and finally falls to smaller values at very large indenter angles. Bishop *et al.* (1945) found that the hardness values decrease up to a certain value and then remain constant for any further increase in indenter angle. Atkins and Tabor, however, found that for material in the fully work hardened state and having a high value of E/σ_y, the initial decrease is followed by a continuous increase in hardness at larger indenter angles.

As indicated by eqn (3), the stress for purely elastic indentations decreases as the cone becomes shallower (larger θ); thus it seems that the decrease in H/σ_y for all materials can be partly attributed to the elastic effect. This is particularly true for silicon (curve a) which, being very hard, will be subjected to larger elastic effects. For a material without strain hardening and with a high value of E/σ_y (curve d), the elastic effect is relatively small and it is necessary to examine how this fully plastic material will deform under the very complex stresses under the indenter. The material which does not strain harden presumably gives rise to a "pile-up" near the indenter, whereas the same material in the annealed condition

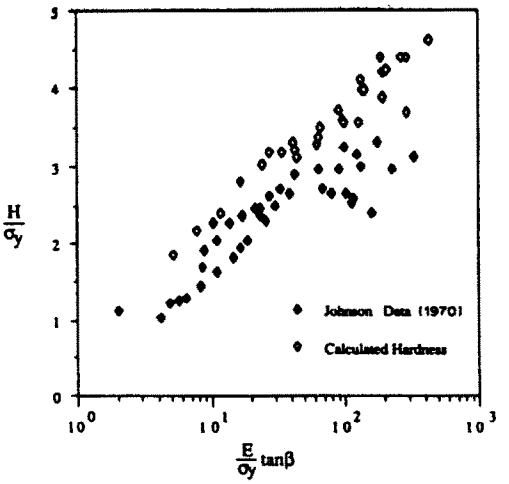

Fig. 14. Comparison of calculated hardness with Johnson's model for various indentation angles.

sinks in due to the strain hardening that occurs during indentation. At smaller cone angles, the mode of deformation is as if the indenter cuts into the material and in this region it seems that the elastic effect, along with the "sink-in" effect, contributes to the decrease in hardness (curve b). For the material without strain hardening, on the other hand, the rate of decrease of the hardness is smaller (curve c). Eventually, for larger cone angles, the mode of deformation changes to one of radial compression. Here, we observe that the hardness increases slightly for the materials that show no strain hardening (curves c and d), whereas for annealed material that exhibits strain hardening during indentation, the decrease in hardness still continues. The probable cause of the continual decrease in hardness for the latter case is due to the effect of the radial compressive mode of deformation which, as suggested by Johnson (1970), maintains compatibility between the volume of material displaced by the indenter and the radial expansion under the indenter. But for the materials without strain hardening, this effect is likely to be offset by the accompanying "pile-up" effect, thus causing an increase in the hardness. At very large cone angles, one observes another drop in hardness, for which a probable explanation first suggested by Atkins and Tabor (1965) may be given as follows. For a cone having such a large angle, the plastic strains produced under the indenter may be of the same order of magnitude as the elastic strains in the more remote regions and due to this effect, the material under the indenter does not experience the complete constraint in plastic flow, thus reducing the hardness.

We have replotted some of these hardness values in Fig. 14 along with the experimental results compiled by Johnson (1970), which are valid only for shallow indenters (i.e. small β). Clearly, the results for small cone angles "θ" (i.e. large β) for materials with high values of E/σ_y are higher than the plateau portion of the Johnson data, thus again indicating a mode of deformation completely different from either radial compression or rigid plastic. All other values lie as an upper bound to the experimental values. These calculated values are expected to be closer to the experimental values if one considers the elastic effect of the indenter.

As a further look at the mode of deformation with a commonly used indenter angle, Fig. 15 shows the plastic zones developed by an indenter having an included angle of 136° and for materials with three different E/σ_y values; $E/\sigma_y = 28.8$ for silicon, 157.1 for an aluminum alloy and 733.3 for silver. From this comparison, it is seen that the shapes of the plastic zones are different for different values of E/σ_y. For the very high value of E/σ_y, the classical theoretical approach is to consider the plastic zone as a rigid plastic (Fig. 4a) slip line field, whereas this is precisely the region where the deformation mode is completely different from the assumed field and rather resembles radial compression. For the intermediate value of E/σ_y, the deformation seems to approximate a combination of radial and cylindrical compression and for the smallest value, it deviates from radial compression.

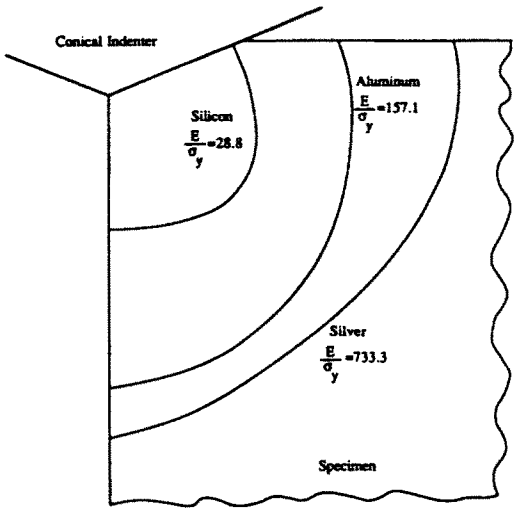

Fig. 15. Comparison of the yield zones at a particular indenter angle of 136° for various E/σ_y ratios for a depth of indentation of 203 nm.

CONCLUSIONS

It is concluded from these FEM simulations that the shapes of the plastic zones for an elastic–plastic solid under a conical indenter strongly depend on the ratio E/σ_y and the indenter angle. These shapes sometimes differ from the predicted hemispherical shapes of the Johnson model and always differ from those assumed in the slip line theory. Specific effects of separately changing the bulk and shear moduli have been studied by applying FEM analysis to conical indentations. It has been found that the bulk modulus has a stronger effect on the hardness of a hard material than the shear modulus, whereas a soft material is more affected by the change in shear modulus than the change in bulk modulus. Predicted hardness variations with indenter angle follow trends observed experimentally for both hard and soft materials under both annealed and work hardened conditions.

Acknowledgements—The authors wish to thank the Defense Research Projects Agency for financial support through the University Research Initiative Program at UCSB under ONR contract N00014-86-K-0753. The authors are also grateful to D. Dungan of the Center of Design Research at Stanford University for his assistance in the use of their IBM4341 computer system.

REFERENCES

ABAQUS finite element program (1985). HKS Inc., Providence, RI.
Atkins, A. G. and Tabor, D. (1965). *J. Mech. Phys. Solids* **13**, 1491.
Bhattacharya, A. K. and Nix, W. D. (1988a). *Int. J. Solids Struct.* **24**, 881.
Bhattacharya, A. K. and Nix, W. D. (1988b). *Int. J. Solids Struct.* **24**, 1287.
Bishop, R. F., Hill, R. and Mott, N. F. (1945). *Proc. Phys. Soc.* **57**, 147.
Bourcier, R. J., Stone, C. M. and Yost, F. G. (1985). Sandia Report No. SAND85-0486.
Dugdale, D. S. (1954). *J. Mech. Phys. Solids* **2**, 265.
Hill, R., Lee, E. H. and Tupper, S. J. (1947). *Proc. R. Soc.* **A188**, 273.
Hill, R., Lee, E. H. and Tupper, S. J. (1951). *Trans. ASME, J. Appl. Mech.* **18**, 46.
Ishlinsky, A. (1944). *J. Appl. Math. Mech.* **8**, 201.
Johnson, K. L. (1970). *J. Mech. Phys. Solids* **18**, 115.
Lee, C. H. and Kobayashi, S. (1970). *Int. J. Mech. Sci.* **12**, 349.
Lee, C. H., Masaki, S. and Kobayashi, S. (1972). *Int. J. Mech. Sci.* **14**, 417.
Lockett, F. J. (1963). *J. Mech. Phys. Solids* **11**, 345.
Marsch, D. M. (1964). *Proc. R. Soc.* **A279**, 420.
Prandtl, L. (1920). *Nachr. Ges. Wiss.*, Gottingen, Math. phys. Kl., 74.
Rubenstein, C. (1981). *J. Appl. Mech.* **48**, 796.
Samuels, L. E. and Mulhearn, T. O. (1957). *J. Mech. Phys. Solids* **5**, 125.
Shield, R. T. (1955). *Proc. R. Soc.* **A233**, 267.
Sneddon, I. N. (1951). *Fourier Transforms*, p. 125. McGraw-Hill, New York.
Tabor, D. (1970). *Rev. Phys. Tech.* **1**, 145.